Signal Processing 125 (2016) 79–86

Contents lists available at ScienceDirect

Signal Processing

journal homepage: www.elsevier.com/locate/sigpro

Fast communication

Real-valued DOA estimation for spherical arrays using sparse Bayesian learning

Qinghua Huang *, Guangfei Zhang, Yong Fang

Key Laboratory of Specialty Fiber Optics and Optical Access Networks, Shanghai University, Shanghai 200072, China

ARTICLE INFO

Article history:
Received 17 September 2015
Received in revised form
13 January 2016
Accepted 14 January 2016
Available online 26 January 2016

Keywords:
Spherical array
Direction-of-arrival (DOA)
Unitary transformation
Variational sparse Bayesian learning (VSBL)

ABSTRACT

Spherical arrays have many advantages for direction-of-arrival (DOA) estimation in 3D space. In this paper, a new real-valued method is proposed to estimate DOAs for spherical arrays. It exploits the property of the complex conjugate of spherical harmonics to find a unitary matrix which can transform the complex array steering matrix into a real matrix. Based on the unitary transformation, a new real-valued array model is constructed to keep the same dimension as the complex-valued model. Then variational sparse Bayesian learning (VSBL) is used to model the joint sparsity between the real part and imaginary part of original data. We get the approximate posterior of the sparse components. The real-valued DOA estimation method acquires good estimation performance and simultaneously decreases the computational cost considerably. Simulation results demonstrate the performance of the proposed method.

© 2016 Elsevier B.V. All rights reserved.

1. Introduction

Direction-of-arrival (DOA) estimation is an important topic in array signal processing and has been widely used in many fields such as radar, sonar, communication, and acoustic system [1,2]. The classical subspace methods, including multiple signal classification (MUSIC) [3] and estimating signal parameter via rotational invariance techniques (ESPRIT) [4], require multi-dimensional search or a special structure of the array. They cannot provide high accuracy. With the development of compressed sensing and sparse reconstruction, the sparse recovery methods have gotten a lot of attentions in DOA estimation due to its high accuracy. Tian et al. used sparse representation and l_0-norm approximation to estimate the DOA and power [5]. However, the l_0-norm needs to be approximated by other norms, which degrades the DOA estimation performance. After that, Wipf et al. proposed an empirical Bayesian strategy to handle the sparse recovery problem based on sparse Bayesian learning (SBL) strategy [6], which is one kind of the most widely researched sparse recovery methods. In order to handle the multitask problem, a multitask compressive sensing method was proposed [7]. Liu et al. proposed a maximum likelihood method for DOA estimation via multiple measurement vector (MMV) SBL which only gave the coarse locations of the sources [8] and then put forward a unified framework to address the DOA estimation problem with typical perturbations of mutual coupling [9]. A refined 1D searching was used to estimate the source directions based on the sparse recovery results. It has a slow convergence rate when the signal-to-noise ratio (SNR) decreases. Zhang et al. put forward a MMV SBL method and gave two suboptimal solutions based on single measurement vector (SMV) and multitask Bayesian compressive sensing [10]. Their method decreased the computational complexity, but the DOA estimation was still processed in the complex number field. In order to deal with the DOA estimation in the real number field, Carlin et al. constructed a general real-valued DOA estimation model for any array structure

* Corresponding author. Tel.: +86 2156337892; fax: +86 2156336908.
E-mail address: qinghua@shu.edu.cn (Q. Huang).

http://dx.doi.org/10.1016/j.sigpro.2016.01.009
0165-1684/© 2016 Elsevier B.V. All rights reserved.

[11]. However, they just combined both the real part and imaginary part directly, so the computational cost cannot be decreased. Moreover, they processed the real part and imaginary part separately without considering the joint sparsity between them. The real part and imaginary part are not in the same rows, so the block sparsity cannot be used directly. Wu et al. kept the joint sparsity between real part and imaginary part by imposing a same weight parameter on them [12]. By using the l_1-norm constraint and singular value decomposition (SVD), Dai et al. proposed a real-valued l_1-SVD method for uniform linear arrays (ULAs) in order to reduce the amount of computations [13]. Then they presented two methods based on l_1-SVD and SBL for DOA estimation using ULAs considering the mutual coupling between the sensor elements [14,15]. However, as mentioned above, they all use ULAs, so the elevation and azimuth of a source cannot be estimated at the same time.

Spherical arrays have spatial symmetrical geometry configurations to capture 3D wave-field information and are widely used in source localization [16,17]. Most of the complex-valued (CV) sparse reconstruction approaches used for ULAs can be extended to estimate DOAs with spherical arrays. However, the number of spherical array sensors is larger than that of ULAs and the dimension of the measurement matrix is much higher than that of ULAs. So the DOA estimation using spherical arrays will require a large amount of computations especially based on the complex-valued model. If the complex-valued model is separated into independent real part and imaginary part, the dimension of the array model will become twice of the original dimension so the DOA estimation still needs a large computational cost. What is more, a localization performance penalty cannot be avoided due to the destroyed joint sparsity between the real part and imaginary part. Besides, the steering matrix of DOA estimation using spherical arrays does not have the centrohermitian property, so the existing real-valued DOA estimation methods for ULAs cannot be directly used for spherical arrays. In order to get a good DOA estimation performance with low amount of computations using spherical arrays, we propose a new real-valued signal model and DOA estimation method. The spherical harmonics decomposition and the property of spherical harmonics are utilized to derive a new real-valued steering matrix. The sparsity of the real part and imaginary part of original data is jointly modeled using the variational SBL (VSBL) method to improve the DOA estimation performance. The proposed method can considerably reduce the computation time.

2. Real-valued spherical array model

The coordinate in Fig. 1 is used to describe the positions of array sensors and sources throughout this paper. We consider a spherical array with the radius R made of L isotropic elements based on the assumption of no mutual coupling between the elements. The position of the lth sensor of the array in the Cartesian coordinate is $\mathbf{R}_l=[R\cos\phi_l\sin\theta_l, R\sin\phi_l\sin\theta_l, R\cos\theta_l]^T$, where θ_l and ϕ_l represent the elevation and azimuth of the lth sensor, respectively. Assuming the dth narrowband far-field signal $s_d(t)$ with the wave vector $\mathbf{k}_d=-[k\sin\vartheta_d\cos\varphi_d, k\sin\vartheta_d\sin\varphi_d, k\cos\vartheta_d]^T$ impinges on the array from $\Phi_d=(\vartheta_d,\varphi_d)$, where k is the wavenumber, ϑ_d and φ_d are the incident elevation and azimuth, respectively, $d=1,\cdots,D$. The array model can be described as

$$\mathbf{x}(t)=\sum_{d=1}^{D}\mathbf{a}_d s_d(t)+\mathbf{v}(t)=\mathbf{A}\mathbf{s}(t)+\mathbf{v}(t), \tag{1}$$

where $\mathbf{x}(t)=[x_1(t),\cdots,x_L(t)]^T\in\mathcal{C}^{L\times 1}$ is the output vector, $\mathbf{v}(t)=[v_1(t),\cdots,v_L(t)]^T\in\mathcal{C}^{L\times 1}$ is the additive white Gaussian noise vector, $\mathbf{s}(t)=[s_1(t),\cdots,s_D(t)]^T\in\mathcal{C}^{D\times 1}$ is the signal vector, t is the snapshot index, and $\mathbf{a}_d=[a(1,d),\cdots,a(L,d)]^T=[e^{-i\mathbf{k}_d^T\mathbf{R}_1},\cdots,e^{-i\mathbf{k}_d^T\mathbf{R}_L}]^T$ is the dth steering vector whose lth element can be represented in spherical harmonics [16,17] as

$$a(l,d)\cong\sum_{n=0}^{N}\sum_{m=-n}^{n}b_n(kR)[Y_n^m(\Phi_d)]^*Y_n^m(\Omega_l), \tag{2}$$

where $\Omega_l=(\theta_l,\varphi_l)$, Y_n^m is the spherical harmonic with order n and degree m defined in [18], N is the highest order of the spherical harmonics decomposition, $b_n(kR)=4\pi i^n j_n(kR)$ is the far-field mode strength for open spherical arrays, $i=\sqrt{-1}$, $j_n(kR)$ is the n-order Bessel function. According to the spherical harmonics representation in (2), the array steering matrix $\mathbf{A}=[\mathbf{a}_1,\cdots,\mathbf{a}_D]\in\mathcal{C}^{L\times D}$ can be written as

$$\mathbf{A}=\mathbf{Y}(\Omega)\mathbf{B}(k)\mathbf{Y}^H(\Phi), \tag{3}$$

where $\mathbf{Y}(\Omega)$ is an $L\times U$ spherical harmonics matrix given by

$$\mathbf{Y}(\Omega)=\begin{bmatrix} Y_0^0(\Omega_1)Y_1^{-1}(\Omega_1)Y_1^0(\Omega_1)Y_1^1(\Omega_1)\cdots Y_N^N(\Omega_1)\\ Y_0^0(\Omega_2)Y_1^{-1}(\Omega_2)Y_1^0(\Omega_2)Y_1^1(\Omega_2)\cdots Y_N^N(\Omega_2)\\ \vdots\quad\vdots\quad\vdots\quad\vdots\quad\ddots\quad\vdots\\ Y_0^0(\Omega_L)Y_1^{-1}(\Omega_L)Y_1^0(\Omega_L)Y_1^1(\Omega_L)\cdots Y_N^N(\Omega_L)\end{bmatrix}, \tag{4}$$

where $U=(N+1)^2$,$\mathbf{B}(k)$ is a $U\times U$ far-field mode strength matrix

$$\mathbf{B}(k)=diag\{b_0(kR),b_1(kR),b_1(kR),b_1(kR),\cdots,b_N(kR)\}. \tag{5}$$

$\mathbf{Y}(\Phi)$ is a $D\times U$ spherical harmonic matrix which contains the directions of source signals as follows

$$\mathbf{Y}(\Phi)=\begin{bmatrix} Y_0^0(\Phi_1)Y_1^{-1}(\Phi_1)Y_1^0(\Phi_1)Y_1^1(\Phi_1)\cdots Y_N^N(\Phi_1)\\ Y_0^0(\Phi_2)Y_1^{-1}(\Phi_2)Y_1^0(\Phi_2)Y_1^1(\Phi_2)\cdots Y_N^N(\Phi_2)\\ \vdots\quad\vdots\quad\vdots\quad\vdots\quad\ddots\quad\vdots\\ Y_0^0(\Phi_D)Y_1^{-1}(\Phi_D)Y_1^0(\Phi_D)Y_1^1(\Phi_D)\cdots Y_N^N(\Phi_D)\end{bmatrix}. \tag{6}$$

According to (3) and the inverse spherical Fourier transform (SFT) $\mathbf{x}(t)=\mathbf{Y}(\Omega)\mathbf{x}_{\mathrm{SH}}(t)$ and $\mathbf{v}(t)=\mathbf{Y}(\Omega)\mathbf{v}_{\mathrm{SH}}(t)$ [19], (1) can be changed to

$$\mathbf{Y}(\Omega)\mathbf{x}_{\mathrm{SH}}(t)=\mathbf{Y}(\Omega)\mathbf{B}(k)\mathbf{Y}^H(\Phi)\mathbf{s}(t)+\mathbf{Y}(\Omega)\mathbf{v}_{\mathrm{SH}}(t), \tag{7}$$

where $\mathbf{x}_{\mathrm{SH}}(t)\in\mathcal{C}^{U\times 1}$ and $\mathbf{v}_{\mathrm{SH}}(t)\in\mathcal{C}^{U\times 1}$ are the SFT coefficient vectors corresponding to the array output vector and the

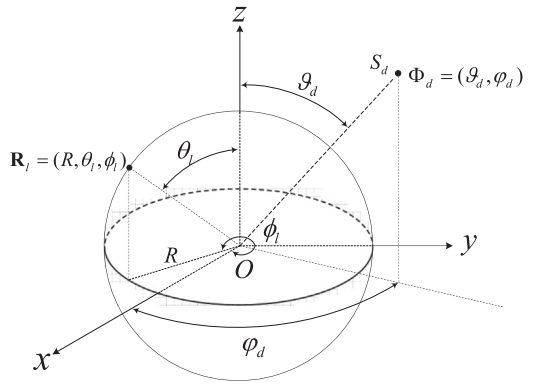

Fig. 1. Spherical coordinate system for localization.

noise vector, respectively. So we get the new CV model in the spherical harmonics domain as follows:

$$\mathbf{x}_{\mathrm{SH}}(t)=\mathbf{A}_{\mathrm{SH}}\mathbf{s}(t)+\mathbf{v}_{\mathrm{SH}}(t), \tag{8}$$

where $\mathbf{A}_{\mathrm{SH}}=\mathbf{B}(k)\mathbf{Y}^H(\Phi)\in\mathcal{C}^{U\times D}$ is the new steering matrix in the spherical harmonics domain. Just like [11], the complex data can be transformed into a direct combination (DC) model as follows:

$$\begin{bmatrix}\mathrm{Re}(\mathbf{x}_{\mathrm{SH}})\\ \mathrm{Im}(\mathbf{x}_{\mathrm{SH}})\end{bmatrix}=\begin{bmatrix}\mathrm{Re}(\mathbf{A}_{\mathrm{SH}}) & -\mathrm{Im}(\mathbf{A}_{\mathrm{SH}})\\ \mathrm{Im}(\mathbf{A}_{\mathrm{SH}}) & \mathrm{Re}(\mathbf{A}_{\mathrm{SH}})\end{bmatrix}\begin{bmatrix}\mathrm{Re}(\mathbf{s})\\ \mathrm{Im}(\mathbf{s})\end{bmatrix}+\begin{bmatrix}\mathrm{Re}(\mathbf{v}_{\mathrm{SH}})\\ \mathrm{Im}(\mathbf{v}_{\mathrm{SH}})\end{bmatrix}, \tag{9}$$

where $\mathrm{Re}(\cdot)$ and $\mathrm{Im}(\cdot)$ represent the real part and imaginary part of a complex value, respectively. This just combines the real part and imaginary part separately and ignores the joint sparsity between them. Moreover, it does not reduce the computational load. Motivated by the approach in [13], we analysis the structure of the new steering matrix by exploring the property of spherical harmonics. Because the complex conjugate of the spherical harmonic has the property of $[Y_n^m(\Phi)]^*=(-1)^m Y_n^{-m}(\Phi)$ [17], the element $a_n^m(\Phi)=b_n(kR)[Y_n^m(\Phi)]^*$ of the new steering matrix $\mathbf{A}_{\mathrm{SH}}$ keeps the similar property as

$$[a_n^m(\Phi)]^*=(-1)^{m+n}a_n^{-m}(\Phi). \tag{10}$$

This property can be exploited to construct a real-valued model.

Let $\mathbf{Q}_0=1$ and define a $(2n+1)\times(2n+1)$ unitary matrix for $n\geq 1$ as follows:

$$\mathbf{Q}_n=\frac{1}{\sqrt{2}}\begin{bmatrix}\mathbf{I}_n & \mathbf{0}_n & \mathbf{J}_n\mathbf{G}_n\\ \mathbf{0}_n^T & i^n\sqrt{2} & \mathbf{0}_n^T\\ -i\mathbf{J}_n & \mathbf{0}_n & i\mathbf{G}_n\end{bmatrix}, \tag{11}$$

where $\mathbf{I}_n$ is an $n\times n$ identity matrix, $\mathbf{J}_n$ stands for an $n\times n$ matrix with ones on its anti-diagonal positions and zeros elsewhere, $\mathbf{0}_n$ represents a column vector containing n zeros, and $\mathbf{G}_n$ is an $n\times n$ diagonal matrix as

$$\mathbf{G}_n=\mathrm{diag}\left\{(-1)^{n+1},\ldots,(-1)^{2n}\right\}. \tag{12}$$

We can construct a block diagonal matrix

$$\mathbf{Q}=\mathrm{blkdiag}\{\mathbf{Q}_0,\ldots,\mathbf{Q}_N\}. \tag{13}$$

$\mathbf{Q}$ is a unitary matrix, *i.e.*, $\mathbf{Q}^{-1}=\mathbf{Q}^H$. Multiplying (8) using the unitary transformation (UT) matrix $\mathbf{Q}$ from the left, we get

$$\mathbf{Q}\mathbf{x}_{\mathrm{SH}}(t)=\mathbf{Q}\mathbf{A}_{\mathrm{SH}}\mathbf{s}(t)+\mathbf{Q}\mathbf{v}_{\mathrm{SH}}(t). \tag{14}$$

The snapshot index t is omitted for the following concise representation. Define $\bar{\mathbf{x}}_{\mathrm{SH}}=\mathbf{Q}\mathbf{x}_{\mathrm{SH}}$,$\bar{\mathbf{v}}_{\mathrm{SH}}=\mathbf{Q}\mathbf{v}_{\mathrm{SH}}$, and a matrix $\bar{\mathbf{A}}=\mathbf{Q}\mathbf{A}_{\mathrm{SH}}=\mathbf{Q}\mathbf{B}(k)\mathbf{Y}^H(\Phi)=[\bar{\mathbf{a}}_1,\ldots,\bar{\mathbf{a}}_D]\in\mathcal{R}^{U\times D}$ which has the same dimension as that of the complex-valued steering matrix $\mathbf{A}_{\mathrm{SH}}$ in the spherical harmonics domain. According to the definitions of the unitary matrix $\mathbf{Q}$ and the far-field mode strength matrix $\mathbf{B}(k)$,the element $\bar{a}_n^m(\Phi_d)$ of the new real-valued steering matrix $\bar{\mathbf{A}}$ can be expressed as follows:

$$\bar{a}_n^m(\Phi_d)=\begin{cases}4\pi\sqrt{2}j_n(kR)\mathrm{Re}\{i^n[Y_n^m(\Phi_d)]^*\}, & m<0,\\ (-1)^n 4\pi j_n(kR)Y_n^m(\Phi_d), & m=0,\\ (-1)^{n+m+1}4\pi\sqrt{2}j_n(kR)\mathrm{Im}\{i^n[Y_n^m(\Phi_d)]^*\}, & m>0.\end{cases} \tag{15}$$

$\bar{\mathbf{x}}_{\mathrm{SH}}$,$\mathbf{s}$, and $\bar{\mathbf{v}}_{\mathrm{SH}}$ can be partitioned into real parts and imaginary parts which are combined as $\bar{\mathbf{X}}=[\mathrm{Re}(\bar{\mathbf{x}}_{\mathrm{SH}}),\ \mathrm{Im}(\bar{\mathbf{x}}_{\mathrm{SH}})]$,$\bar{\mathbf{S}}=[\mathrm{Re}(\mathbf{s}),\ \mathrm{Im}(\mathbf{s})]$, and $\bar{\mathbf{V}}=[Re(\bar{\mathbf{v}}_{\mathrm{SH}}),\ \mathrm{Im}(\bar{\mathbf{v}}_{\mathrm{SH}})]$. The CV model in (14) can be transformed into a real-valued model as

$$\bar{\mathbf{X}}=\bar{\mathbf{A}}\bar{\mathbf{S}}+\bar{\mathbf{V}}. \tag{16}$$

Now, the real part and imaginary part are in the same rows which provide the condition for using their sparsity jointly.

3. DOA estimation using VSBL

In order to estimate DOAs by sparse recovery method, we sample the potential azimuth and elevation space of the incident signals to form a DOA set $\boldsymbol{\Theta}=\{\Theta_1,\cdots,\Theta_J\}=\{(\bar{\vartheta}_1,\bar{\varphi}_1),\cdots,(\bar{\vartheta}_J,\bar{\varphi}_J)\}$. The measurement matrix is $\tilde{\mathbf{A}}=[\bar{\mathbf{a}}_1,\ldots,\bar{\mathbf{a}}_J]\in\mathcal{R}^{U\times J}$, where$J>>U>D$. For Q snapshots, the multiple measurement vector (MMV) model can be written as

$$\tilde{\mathbf{X}}=\tilde{\mathbf{A}}\tilde{\mathbf{S}}+\tilde{\mathbf{V}}, \tag{17}$$

where $\tilde{\mathbf{X}}\in\mathcal{R}^{U\times 2Q}$,$\tilde{\mathbf{S}}\in\mathcal{R}^{J\times 2Q}$, and $\tilde{\mathbf{V}}\in\mathcal{R}^{U\times 2Q}$.The sparse matrix $\tilde{\mathbf{S}}$ has non-zero rows only corresponding to the true source directions. We model $\tilde{\mathbf{S}}$ as hidden variable and use variational Bayesian method to approximate the posterior distributions of the hidden variables and then update the distribution parameters [20]. A two-level hierarchical matrix normal prior is imposed on the sparse matrix $\tilde{\mathbf{S}}$

$$p(\tilde{\mathbf{S}}|\boldsymbol{\beta})=\mathcal{MN}_{J,2Q}(\mathbf{0},\boldsymbol{\beta},\mathbf{I}_{2Q})=(2\pi)^{-JQ}|\boldsymbol{\beta}|^{Q}\exp\left(-0.5\mathrm{tr}[\tilde{\mathbf{S}}^T\boldsymbol{\beta}\tilde{\mathbf{S}}]\right), \tag{18}$$

and

$$p(\beta_j)=\Gamma(\beta_j|b^{(\beta)},c^{(\beta)}), \tag{19}$$

where $\boldsymbol{\beta}=\mathrm{diag}\{\beta_1,\cdots,\beta_J\}$, $\Gamma(\cdot|a,b)$ denotes the Gamma distribution with the parameters a and b, and $\mathrm{tr}(\cdot)$ denotes the trace of a matrix. The noise can be approximately modeled as Gaussian with zero-mean and the variance

equal to γ^{-1} as

$$p(\tilde{\mathbf{V}}|\gamma)=\mathcal{MN}_{U,2Q}(\mathbf{0},\gamma\mathbf{I}_U,\mathbf{I}_{2Q}) \tag{20}$$

with $p(\gamma)=\Gamma(\gamma|b^{(\gamma)},c^{(\gamma)})$.

Variational Bayesian inference minimizes the Kullback–Leibler (KL) divergence which measures the difference of the probability mass between the approximate probability density function (pdf) $q(\tilde{\mathbf{S}},\boldsymbol{\beta},\gamma)$ and its posterior $p(\tilde{\mathbf{S}},\boldsymbol{\beta},\gamma|\tilde{\mathbf{X}})$. Since $p(\tilde{\mathbf{S}},\boldsymbol{\beta},\gamma|\tilde{\mathbf{X}})$ is usually intractable, an alternative approach is to use variational expectation maximization (EM) strategy [20,21] to minimize the cost function

$$\mathrm{C_{KL}}=\left\langle \log\frac{q(\tilde{\mathbf{S}},\boldsymbol{\beta},\gamma)}{p(\tilde{\mathbf{S}},\boldsymbol{\beta},\gamma,\tilde{\mathbf{X}})}\right\rangle_q=\left\langle \log\frac{q(\tilde{\mathbf{S}})q(\boldsymbol{\beta})q(\gamma)}{p(\tilde{\mathbf{X}}|\tilde{\mathbf{S}},\boldsymbol{\beta},\gamma)p(\tilde{\mathbf{S}}|\boldsymbol{\beta})p(\boldsymbol{\beta})p(\gamma)}\right\rangle_q, \tag{21}$$

where $\left\langle\tilde{\mathbf{S}}\right\rangle_q$ denotes the expectation of $\tilde{\mathbf{S}}$ under its distribution $q(\tilde{\mathbf{S}})$.

In the variational E-step, $q(\tilde{\mathbf{S}})$ is updated according to $q(\tilde{\mathbf{S}})\propto exp\left(\left\langle\log p(\tilde{\mathbf{X}},\tilde{\mathbf{S}}|\boldsymbol{\beta},\gamma)\right\rangle_q\right)$. According to the distributions $p(\tilde{\mathbf{X}}|\tilde{\mathbf{S}},\gamma)$ and $p(\tilde{\mathbf{S}}|\boldsymbol{\beta})$, the joint distribution can be described as $p(\tilde{\mathbf{X}},\tilde{\mathbf{S}}|\boldsymbol{\beta},\gamma)=p(\tilde{\mathbf{X}}|\tilde{\mathbf{S}},\gamma)p(\tilde{\mathbf{S}}|\boldsymbol{\beta})$. Therefore, we can get the approximate posterior density for $\tilde{\mathbf{S}}$ as

$$q(\tilde{\mathbf{S}})=\mathcal{MN}_{J,2Q}(\mathbf{U},\boldsymbol{\Sigma},\mathbf{I}_{2Q}). \tag{22}$$

The parameters of the approximate posterior in (22) can be updated according to

$$\boldsymbol{\Sigma}=\langle\gamma\rangle_q\tilde{\mathbf{A}}^T\tilde{\mathbf{A}}+\langle\boldsymbol{\beta}\rangle_q, \tag{23}$$

$$\mathbf{U}=\langle\gamma\rangle_q\boldsymbol{\Sigma}^{-1}\tilde{\mathbf{A}}^T\tilde{\mathbf{X}}. \tag{24}$$

In the variational M-step, $q(\boldsymbol{\beta},\gamma)$ is updated according to $q(\boldsymbol{\beta},\gamma)\propto p(\boldsymbol{\beta},\gamma)exp\left(\left\langle\log p(\tilde{\mathbf{X}},\tilde{\mathbf{S}}|\boldsymbol{\beta},\gamma)\right\rangle_q\right)$. Assuming all the parameters in $\boldsymbol{\beta}$ and γ are mutually independent, the joint prior for $\boldsymbol{\beta}$ and γ can be expressed as $p(\boldsymbol{\beta},\gamma)=p(\gamma)\sum_{j=1}^{J}p(\beta_j)$. The optimal approximating distributions for all the parameters are given by

$$q(\beta_j)=\Gamma(\beta_j|\bar{b}_j^{(\beta)},\bar{c}_j^{(\beta)}), \tag{25}$$

$$q(\gamma)=\Gamma(\gamma|\bar{b}^{(\gamma)},\bar{c}^{(\gamma)}). \tag{26}$$

The average for β_j^{-1} under its posterior is $\langle\beta_j\rangle_q^{-1}=\bar{b}_j^{(\beta)}/\bar{c}_j^{(\beta)}$. It controls the sparsity of $\tilde{\mathbf{S}}_{j,:}$, where $\tilde{\mathbf{S}}_{j,:}$ denotes the jth row entry of $\tilde{\mathbf{S}}$. In practice, a small pruning threshold is set for the sparsity parameter $\langle\beta_j\rangle_q^{-1}$. During the iteration learning, when $\langle\beta_j\rangle_q^{-1}$ is less than the small pruning threshold, the corresponding basis function $\bar{\mathbf{a}}_j$ is removed from the dictionary $\tilde{\mathbf{A}}(\boldsymbol{\Theta})$. The updating equations for the approximate posterior parameters of these precisions are written as

$$\bar{c}_j^{(\beta)}=c^{(\beta)}+Q, \tag{27}$$

$$\bar{b}_j^{(\beta)}=b^{(\beta)}+0.5\left\langle\tilde{\mathbf{S}}_{j,:}\tilde{\mathbf{S}}_{j,:}^T\right\rangle_q. \tag{28}$$

The approximate posterior parameters $\bar{c}^{(\gamma)}$ and $\bar{b}^{(\gamma)}$ can be updated as

$$\bar{c}^{(\gamma)}=c^{(\gamma)}+UQ, \tag{29}$$

$$\bar{b}^{(\gamma)}=b^{(\gamma)}+0.5tr\left[\left\langle(\tilde{\mathbf{X}}-\tilde{\mathbf{A}}\tilde{\mathbf{S}})^T(\tilde{\mathbf{X}}-\tilde{\mathbf{A}}\tilde{\mathbf{S}})\right\rangle_q\right]. \tag{30}$$

The variational Bayesian learning has excellent performance in terms of the sparse recovery. When the algorithm converges, the DOAs are chosen from the DOA set $\boldsymbol{\Theta}$ according to the indexes of the D non-zero rows in the sparse matrix $\mathbf{U}$.

We compare the CV model (8), the DC model (9), and the UT model (16) using the same VSBL method, which are named CV-VSBL, DC-VSBL, and UT-VSBL, respectively. UT-VSBL has the following two advantages.

3.1. The DOA estimation performance

The CV-MMV sparse model is expressed as $\tilde{\mathbf{X}}_c=\tilde{\mathbf{A}}_c\tilde{\mathbf{S}}_c+\tilde{\mathbf{V}}_c$. The DC method models $p(\mathrm{Re}(\tilde{\mathbf{S}}_c)|\boldsymbol{\beta}_1)$, $p(\mathrm{Im}(\tilde{\mathbf{S}}_c)|\boldsymbol{\beta}_2)$, $p(\mathrm{Re}(\tilde{\mathbf{V}}_c)|\gamma_1)$, and $p(\mathrm{Im}(\tilde{\mathbf{V}}_c)|\gamma_2)$ independently in VSBL. This ignores the joint sparsity of the real part and imaginary part. Compared with it, UT-VSBL method keeps the real part and imaginary part in the same rows so that the joint sparsity between them can be used to estimate source DOAs. In (23), (24), (28), and (30), $\tilde{\mathbf{A}}^T\tilde{\mathbf{A}}=\tilde{\mathbf{A}}_c^H\tilde{\mathbf{A}}_c$,$\tilde{\mathbf{A}}^T\tilde{\mathbf{X}}=\tilde{\mathbf{A}}_c^H\tilde{\mathbf{X}}_c$, $\tilde{\mathbf{S}}_{j,:}\tilde{\mathbf{S}}_{j,:}^T=\tilde{\mathbf{S}}_{c(j,:)}\tilde{\mathbf{S}}_{c(j,:)}^H$, and $tr(\tilde{\mathbf{X}}-\tilde{\mathbf{A}}\tilde{\mathbf{S}})^T(\tilde{\mathbf{X}}-\tilde{\mathbf{A}}\tilde{\mathbf{S}})=tr(\tilde{\mathbf{X}}_c-\tilde{\mathbf{A}}_c\tilde{\mathbf{S}}_c)^H(\tilde{\mathbf{X}}_c-\tilde{\mathbf{A}}_c\tilde{\mathbf{S}}_c)$. For CV and UT methods, the different updates only lie in (27) and (29) due to different snapshots, which have little effect on the posterior parameters learning. Moreover, the unitary transformation does not change the energies of signals and noises. Therefore, the DOA estimation using UT model is expected to have a better performance than using the DC model and similar performance to the DOA estimation using the CV model.

3.2. The computational cost

The dimension of the steering matrix using the DC model (9) doubles that of the CV model (8). So the DOA estimation using the DC model costs more time than using the CV model. In variational sparse Bayesian DOA estimation, the dimension J of the measurement matrix is very large. The high dimensional measurement matrix $\tilde{\mathbf{A}}$ affects the parameter updates in (23), (24), and (30) in the iterative learning process. Our method transforms the complex measurement matrix into a real matrix without changing the dimension through a unitary transformation. Therefore, the DOA estimation using the UT model can reduce more than half computational load compared with using the CV model. Table 1 shows the amount of computations using the two models. The amount of computations is assessed in terms of the number of real multiplication (RM) and real addition (RA). One complex multiplication is equivalent to 4 RM and 2 RA and one complex addition is equivalent to 2 RA.

Table 1
Comparison of computational load in one iteration.

Main item		Amount	
		RM	RA
CV model	$\tilde{\mathbf{A}}_c^H\tilde{\mathbf{A}}_c$	$4UJ^2$	$(4U-2)J^2$
	$\tilde{\mathbf{A}}_c^H\tilde{\mathbf{X}}_c$	$4UJQ$	$(4U-2)JQ$
	$\tilde{\mathbf{A}}_c\tilde{\mathbf{S}}_c$	$4UJQ$	$U(4J-2)Q$
UT model	$\tilde{\mathbf{A}}^T\tilde{\mathbf{A}}$	UJ^2	$(U-1)J^2$
	$\tilde{\mathbf{A}}^T\tilde{\mathbf{X}}$	$2UJQ$	$2U(J-1)Q$
	$\tilde{\mathbf{A}}\tilde{\mathbf{S}}$	$2UJQ$	$2(U-1)JQ$

In [16], the ESPRIT method uses the recursive relation of the spherical harmonics to estimate DOA. It is not a sparse recovery method and has low computational complexity. A real-valued model for ULAs was constructed and then l_1-SVD method was used to estimate the DOAs in [13]. We compare the DOA estimation performance of UT-VSBL method with ESPRIT and l_1-SVD method. In terms of computational complexity, the ESPRIT method for spherical arrays is $\mathcal{O}(U^3)$. In general, U is much less than the number of the sparse grids J. For optimizing the objective function in the second-order cone framework using an interior point implementation, the complexity of l_1-SVD is $\mathcal{O}(D^3J^3)$. Compared to these methods, the computational complexity of UT-VSBL is $\mathcal{O}(U^2J)$. From the analysis we can know that the computational complexity of UT-VSBL is larger than the ESPRIT method, and much smaller than the l_1-SVD method especially when J is large. As the DC model doubles the dimension of the UT model, $\overline{U}=2U, \overline{J}=2J$, the complexity of using it becomes $\mathcal{O}(\overline{U}^2\overline{J})$, which of course increases the computational load.

4. Simulations

In this section the radius of open spherical array is chosen as 0.1 m with 32 uniformly distributed sensors. The distance between neighboring samples of the uniform sampling scheme is constant. The uniform sampling scheme gives rise to a limited set of special geometries called platonic solids and it is only possible for certain numbers of sensor elements [22]. The maximum order of the spherical mode is $N=4$. These simulations are performed using MATLAB 2012b running on the Intel i3, 2.66 GHz processor with 4 GB memory, under Win7 system. SVD is used to reduce the amount of computations before the sparse components learning. Therefore, the number of snapshots has little effect on the computational cost. In order to avoid the aliasing error, kR should be less than N, so the frequencies of the signals should be less than 2.16 kHz [22]. If kR is too small, the mode strength $b_n(kR)$ decreases greatly. So in the simulations, the frequencies of source signals are randomly chosen in the range from 1 kHz to 2.15 kHz.

Firstly, we test the time cost of DOA estimation based on different models. The SNR is fixed at 5 dB. Two signals impinge on the spherical array from (35°, 55°) and (70°, 134°). The grid intervals of azimuth and elevation are (10°, 5°), (5°, 2°), and (2°, 1°), respectively. The average time of ten trials are shown in Table 2. The computational time increases quickly as the grid interval becomes small. UT-VSBL method costs the least time because it has the same dimension as the CV model and requires only real operations in sparse recovery. The dimension of the DC model is

Table 2
Comparison of computation time.

Grid intervals of azimuth and elevation (deg)	Time (s)		
	CV-VSBL	DC-VSBL	UT-VSBL
(10,5)	0.27	0.51	0.11
(5,2)	1.22	2.31	0.44
(2,1)	8.43	16.32	2.42

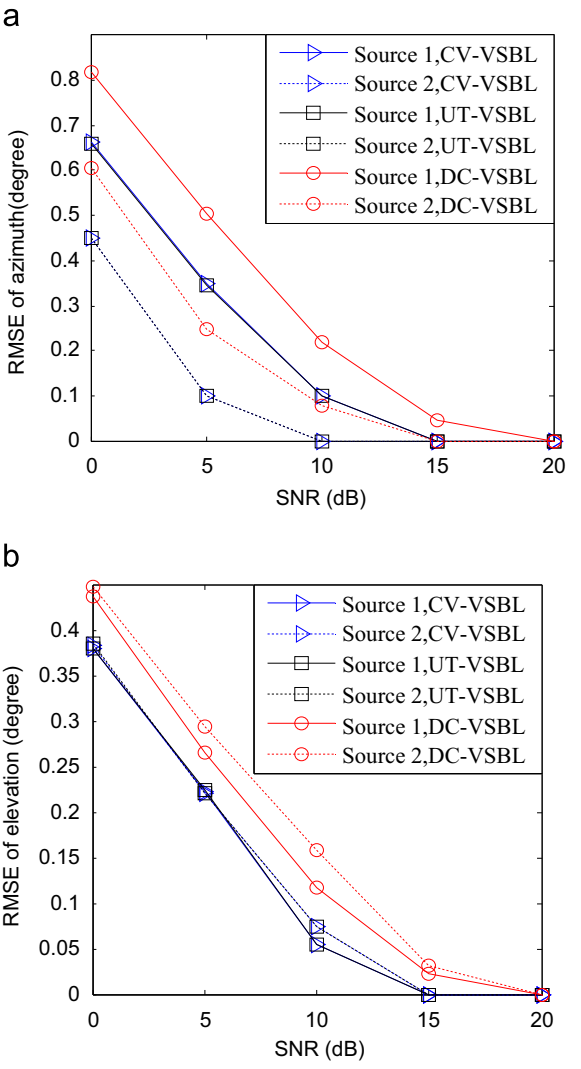

Fig. 2. DOA estimation performance of two sources at (35°, 65°) and (70°, 154°). The figure shows RMSE vs. SNR. (a) RMSE of azimuth and (b) RMSE of elevation.

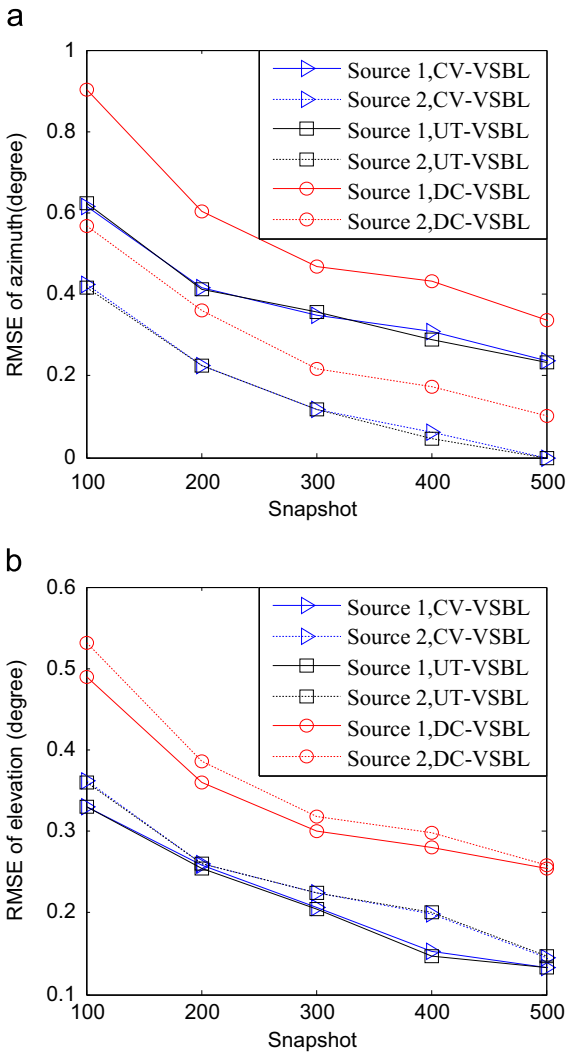

Fig. 3. DOA estimation performance of two sources at (35°, 55°) and (60°, 134°). The figure shows RMSE vs. snapshot. (a) RMSE of azimuth and (b) RMSE of elevation.

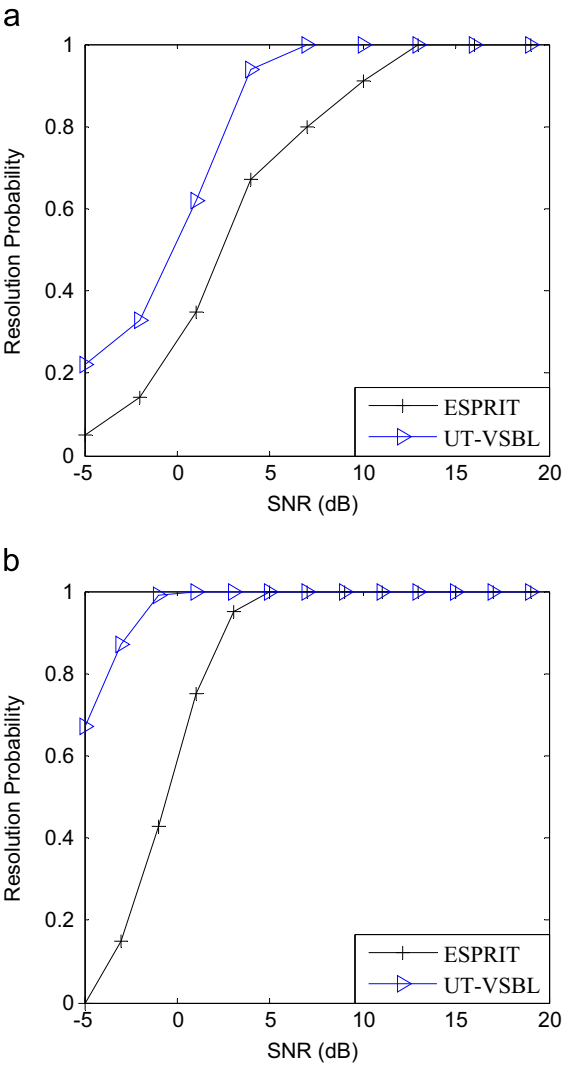

Fig. 4. Resolution probability for two closely spaced sources. The figure shows resolution probability vs. SNR. (a) Resolution probability of azimuth of two sources at (35°, 80°) and (35°, 95°) and (b) resolution probability of elevation of two sources at (35°, 75°) and (45°, 75°).

twice of the original CV model which leads to more parameter updates in the Bayesian learning process. So the DC method costs more time than CV-VSBL method. When the grid intervals are (2°, 1°), we also compare the cost time of UT-VSBL, ESPRIT, and l_1-SVD method. The time costs are 2.48 s, 0.002 s, and 71.50 s, respectively. This shows that our proposed method costs more time than ESPRIT and less time than the l_1-SVD method. However, the computation time of UT-VSBL can be reduced through using a coarse grid at first and then refining it.

Root mean square error (RMSE) is adopted to evaluate the DOA estimation performance of these estimation algorithms. The grid intervals of azimuth and elevation are (1°, 0.5°). SNR varies from 0 dB to 20 dB. The number of snapshots is set as 200. Two uncorrelated far-field narrowband signals impinge on the spherical array from (35°, 65°) and (70°, 154°). The RMSEs of 500 independent Monte Carlo trials are shown in Fig. 2. The results show that UT-VSBL has lower RMSEs than DC-VSBL which ignores the joint sparsity of the real part and imaginary part. Then the SNR is fixed at 5 dB and the number of snapshot varies from 100 to 500 with 500 independent Monte Carlo trials. The bearings of two signals are (35°, 55°) and (60°, 134°). The results are shown in Fig. 3, which also indicate that the performance of UT-VSBL is better due to exploiting the joint sparsity of the real part and imaginary part. The proposed UT model can acquire similar performance as the original CV model because it keeps the energies of signals and noises unchanged.

In this part, we compare the performance of UT-VSBL method with a conventional subspace-based method. Both UT-VSBL method and l_1-SVD are the sparse recovery methods with a high resolution. ESPRIT is one kind of subspace-based method. The resolution power of UT-VSBL is compared with that of ESPRIT. We firstly testify the azimuth resolution power. Two uncorrelated far-field

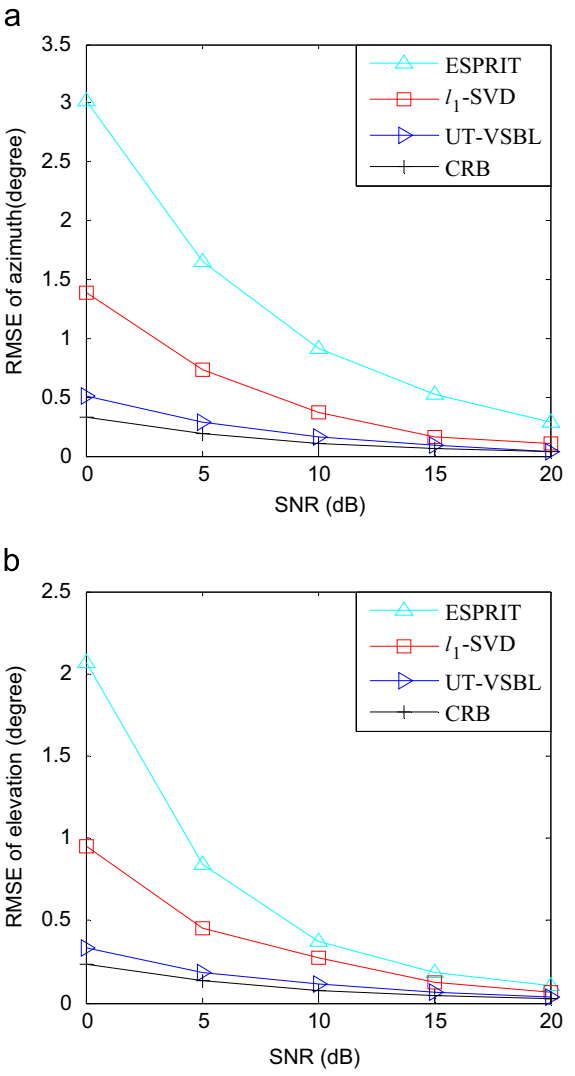

Fig. 5. DOA estimation performance of two sources and CRB at (35°, 55°) and (70°, 154°). The figure shows RMSE and CRB vs. SNR. (a) RMSE of azimuth and (b) RMSE of elevation.

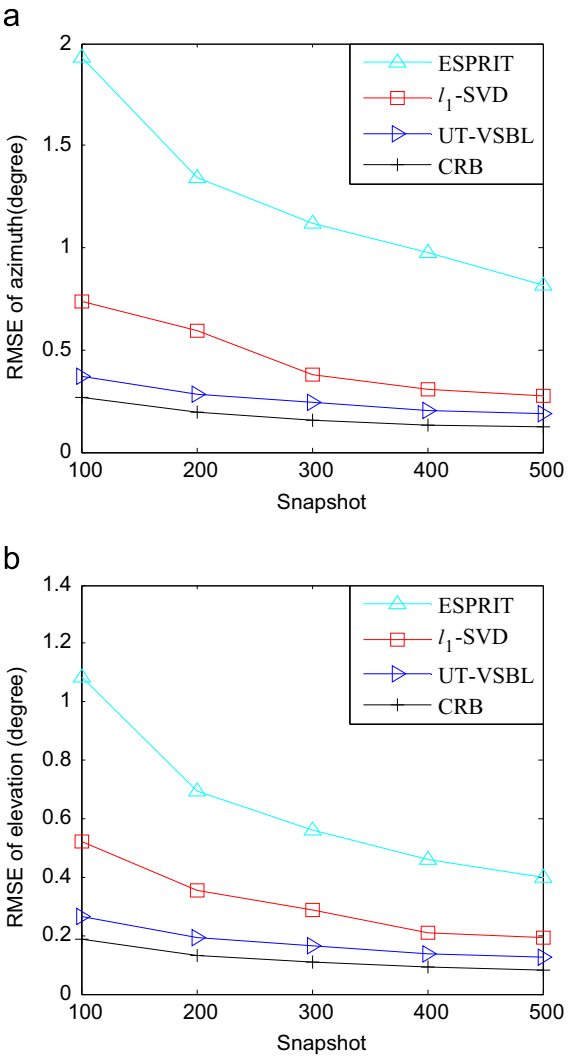

Fig. 6. DOA estimation performance of two sources and CRB at (35°, 55°) and (60°, 134°). The figure shows RMSE and CRB vs. snapshot. (a) RMSE of azimuth and (b) RMSE of elevation.

narrowband signals impinge on the spherical array from (35°, 80°) and (35°, 95°), respectively. According to [13], the two signals are resolved if $\max_{d=1,2}\{|\hat{\varphi}_d-\varphi_d|\}$ is less than $|\varphi_1-\varphi_2|/2$, where $\hat{\varphi}_d$ stands for the estimated azimuth for the dth signal. The grid interval is 0.5°. Through 100 Monte Carlo runs, the resolution probability for azimuth are shown in Fig. 4(a). Then assuming two signals impinge on the spherical array from (35°, 75°) and (45°, 75°), the resolution probability for elevation are shown in Fig. 4(b). The two signals are resolved if $\max_{d=1,2}\{|\hat{\vartheta}_d-\vartheta_d|\}$ is less than $|\vartheta_1-\vartheta_2|/2$, where $\hat{\vartheta}_d$ stands for the estimated elevation for the dth signal. Fig. 4 indicates that our proposed method has a better resolution than the ESPRIT method.

The Cramer Rao bound (CRB) defines the ultimate accuracy of any unbiased estimation procedure. In order to verify the performance of our proposed method, the RMSEs of these different methods are compared to the CRBs. The grid intervals of azimuth and elevation are (0.2°, 0.1°). Firstly, assuming two signals impinge on the spherical array from (35°, 55°) and (70°, 154°), the number of snapshots is set as 200 with SNR changing from 0 dB to 20 dB. Through 500 independent Monte Carlo trials, the RMSEs of UT-VSBL, ESPRIT and l_1-SVD are shown in Fig. 5. Then assuming two signals impinge on the spherical array from (35°, 55°) and (60°, 134°), the SNR is fixed at 5 dB with the number of snapshots changing from 100 to 500. The estimation RMSE results including CRBs are shown in Fig. 6. We can see that UT-VSBL method achieves a better performance than the other methods.

5. Conclusions

In this paper, we construct a new real-valued model for spherical arrays by a unitary transformation. The dimension of the new model is the same as that of the CV model and the joint sparsity between the real part and imaginary

part is exploited in DOA estimation by VSBL method. Simulation results show that our proposed method has similar results as CV-VSBL with a lower amount of computations and it has a better performance than the DC-VSBL, ESPRIT, and l_1-SVD sparse method. For future work, it will be interesting to research the DOA estimation of wideband signals and consider the mutual coupling between the elements of spherical arrays.

Acknowledgment

The authors would like to thank the editor and anonymous reviewers for their valuable comments. This work was supported by National Natural Science Foundation of China (61571279) and Natural Science Foundation of Shanghai (14ZR1415000) of China.

References

[1] H. Krim, M. Viberg, Two decades of array signal processing research: the parametric approach, IEEE Signal Process. Mag. 13 (4) (1996) 67–94.
[2] A. Boukerche, H.A.B. Oliveira, E.F. Nakamura, A.A.F. Loureiro, Localization systems for wireless sensor networks, IEEE Trans. Wirel. Commun. 14 (6) (2007) 6–12.
[3] R.O. Schmidt, Multiple emitter location and signal parameter estimation, IEEE Trans. Antennas Propag. 34 (3) (1986) 276–280.
[4] R. Roy, T. Kailath, ESPRIT-estimation of signal parameters via rotational invariance techniques, IEEE Trans. Acoust. Speech Signal Process. 37 (7) (1989) 984–995.
[5] Y. Tian, X. Sun, S. Zhao, DOA and power estimation using a sparse representation of second-order statistics vector and l_0-norm approximation, Signal Process. 105 (2014) 395–400.
[6] D. Wipf, B. Rao, An empirical Bayesian strategy for solving the simultaneous sparse approximation problem, IEEE Trans. Signal Process. 55 (7) (2007) 3704–3716.
[7] S. Ji, D. Dunson, L. Carin, Multitask compressive sensing, IEEE Trans. Signal Process. 57 (1) (2009) 92–106.
[8] Z. Liu, Z. Huang, Y. Zhou, An efficient maximum likelihood method for direction-of-arrival estimation via sparse bayesian learning, IEEE Trans. Wirel. Commun. 11 (10) (2012) 1–11.
[9] Z. Liu, Y. Zhou, A unified framework and sparse Bayesian perspective for direction-of-arrival estimation in the presence of array imperfections, IEEE Trans. Signal Process. 61 (15) (2013) 3786–3798.
[10] J. Zhang, Z. Chen, P. Cheng, X. Huang, Multiple-measurement vector based implementation for single-measurement vector sparse Bayesian learning with reduced complexity, Signal Process. 118 (2016) 153–158.
[11] M. Carlin, P. Rocca, G. Oliveri, F. Viani, A. Massa, Directions-of-arrival estimation through Bayesian compressive sensing strategies, IEEE Trans. Antennas Propag. 61 (7) (2013) 3828–3837.
[12] Q. Wu, Y. Zhang, M. G. Amin, B. Himed, Complex multitask Bayesian compressive sensing, in: Proceedings of 39th IEEE International Conference on Acoustic Speech and Signal Processing (ICASSP), Florence, Italy, 5, 2014, pp. 3375–3379.
[13] J. Dai, X. Xu, D. Zhao, Direction-of-arrival estimation via real-valued sparse representation, IEEE Antennas Wirel. Propag. Lett. 12 (2013) 376–379.
[14] J. Dai, W. Xu, D. Zhao, J. Dai, Real-valued DOA estimation for uniform linear array with unknown mutual coupling, Signal Process. 92 (2012) 2056–2065.
[15] J. Dai, N. Hu, W. Xu, C. Chang, Sparse Bayesian learning for DOA estimation with mutual coupling, Sensors 15 (2015) 26267–26280.
[16] R. Goossens, H. Rogier, Unitary spherical ESPRIT: 2-D angle estimation with spherical arrays for scalar fields, IET Signal Process. 3 (3) (2009) 221–231.
[17] H. Sun, S. Yan, U.P. Svensson, Robust minimum sidelobe beamforming for spherical microphone arrays, IEEE Trans. Audio Speech Lang. Process. 19 (4) (2011) 1045–1051.
[18] E.G. Williams, Spherical Waves, in Fourier Acoustics: Sound Radiation and Nearfield Acoustical Holography, Academic, New York, 1999, 183–197.
[19] J.R. Driscoll, D.M.H. Computing, Fourier transforms and convolutions on the 2-sphere, Adv. Appl. Mech. 15 (2) (1994) 202–250.
[20] D. Shutin, T. Buchgraber, S.R. Kulkarni, H.V. Poor, Fast variational sparse Bayesian learning with automatic relevance determination for superimposed signals, IEEE Trans. Signal Process. 59 (12) (2011) 6257–6261.
[21] C.W. Fox, S.J. Roberts, A tutorial on variational Bayesian inference, Artif. Intell. Rev. 38 (2) (2012) 85–95.
[22] B. Rafaely, Analysis and design of spherical microphone arrays, IEEE Trans. Speech Audio Process. 13 (1) (2005) 135–143.